KvAP-Based Model of the Pore Region of *Shaker* Potassium Channel Is Consistent with Cadmium- and Ligand-Binding Experiments

Iva Bruhova and Boris S. Zhorov
Department of Biochemistry and Biomedical Sciences, McMaster University, Hamilton, Ontario, Canada

ABSTRACT Potassium channels play fundamental roles in excitable cells. X-ray structures of bacterial potassium channels show that the pore-lining inner helices obstruct the cytoplasmic entrance to the closed channel KcsA, but diverge in widely open channels MthK and KvAP, suggesting a gating-hinge role for a conserved Gly in the inner helix. A different location of the gating hinge and a narrower open pore were proposed for voltage-gated *Shaker* potassium channels that have the Pro-473-Val-Pro motif. Two major observations back the proposal: cadmium ions lock mutant Val-476-Cys in the open state by bridging Cys-476 and His-486 in adjacent helices, and cadmium blocks the locked-open double mutant Val-474-Cys/Val-476-Cys by binding to Cys-474 residues. Here we used molecular modeling to show that the open *Shaker* should be as wide as KvAP to accommodate an open-channel blocker, correolide. We further built KvAP-, MthK-, and KcsA-based models of the *Shaker* mutants and Monte-Carlo-minimized them with constraints Cys-476—Cd^{2+}—His-486. The latter were consistent with the KvAP-based model, causing a small-bend N-terminal to the Pro-473-Val-Pro motif. The constraints significantly distorted the MthK-based structure, making it similar to KvAP. The KcsA structure resisted the constraints. Two Cd^{2+} ions easily block the locked-open KvAP-based model at Cys-474 residues, whereas constraining a single cadmium ion to four Cys-474 caused large conformational changes and electrostatic imbalance. Although mutual disposition of the voltage-sensor and pore domains in the KvAP x-ray structure is currently disputed, our results suggest that the pore-region domain retains a nativelike conformation in the crystal.

INTRODUCTION

Potassium channels are a highly diverse group of integral membrane proteins that play fundamental roles in cell physiology. The channels underlie the electrical activity of cells, being responsible for the maintenance of the resting membrane potential and the propagation of the action potential. Voltage-gated K^+ channels (Kv channels) are involved in the electrical impulse generation in nerve, muscle, endocrine, and other excitable cells. The landmark crystallographic structures of bacterial K^+ channels show that the pore-lining inner helices obstruct the cytoplasmic entrance to the closed channel KcsA (1), but diverge into widely open channels MthK (2) and KvAP (3), suggesting a gating-hinge role for conserved glycine in the inner helix (4). The x-ray structures of bacterial channels helped to explain a large body of experimental data on eukaryotic channels and have been used as templates to build homology models of pharmacologically important voltage-gated potassium (5–7), sodium (8,9), and calcium (10,11) channels, as well as channels gated by glutamate (12) and cyclic nucleotides (13). However, the reliability of the homology models is questioned by controversial interpretations of experiments addressing structural similarity between prokaryotic and eukaryotic K^+ channels.

In the absence of high-resolution structures of eukaryotic channels, information on their geometry is deduced from experiments such as chemical cross-linking, metal binding, ligand binding, and cysteine scanning. These experiments do not provide direct data on the channel geometry, but determine distance constraints between individual atoms and residues. The emerging picture of the pore architecture of Kv channels generally agrees with the structure of bacterial K^+ channels. However, Kv channels have important structural peculiarities within the pore domain. The inner helices of Kv channels include a highly conserved Pro-X-Pro motif between the conserved glycine, which is N-terminal to the motif, and C-terminal residues whose crossover forms the activation gate in bacterial channels. In *Shaker* channels, the Pro-X-Pro motif includes residues Pro-473, Val-474, and Pro-475 referred to as the Pro-473-Val-Pro (PVP) motif. Lu et al. (14) substituted the pore of a prokaryotic channel into a eukaryotic voltage-gated channel and showed that the resulting chimera retained the hallmark functional properties of eukaryotic channels, indicating that the ion conduction pore is conserved among K^+ channels.

A different conclusion regarding the similarity between prokaryotic and eukaryotic K^+ channels has been proposed by Yellen and co-workers. In particular, del Camino et al. (15) demonstrated that intracellularly applied blockers prevent chemical modification of engineered cysteines in the inner helices C-terminal to the PVP motif, but not at the positions N-terminal to it. To explain this fact, the authors hypothesized that, unlike prokaryotic channels, the *Shaker* channels have a sharp bend at the PVP motif. This

Submitted March 2, 2005, and accepted for publication May 17, 2005.

Address reprint requests to Boris S. Zhorov, Dept. of Biochemistry and Biomedical Sciences, McMaster University, 1200 Main St. W., Hamilton, ON, L8N 3Z5 Canada. Tel.: 905-525-9140 ext. 22049; Fax: 905-522-9033; E-mail: zhorov@mcmaster.ca.

0006-3495/05/08/1020/10 $2.00

doi: 10.1529/biophysj.105.062240

hypothesis is supported by the seminal studies of Cd^{2+} action on *Shaker* mutants (16,17), which provided valuable distance constraints between certain residues in the inner helices of the open *Shaker* channel. The authors found that 1), Cd^{2+} ions lock mutant Val-476-Cys in the open state by bridging Cys-476 and His-486 in adjacent helices; and 2), Cd^{2+} blocks the locked-open double mutant Val-474-Cys/Val-476-Cys by coordinating Cys-474 residues. Current structural interpretation of these constraints is visualized in a conceptual model, in which the N-terminal halves of the inner helices are disposed as in KcsA to form a rather narrow open pore, whereas the C-terminal halves kink significantly at the PVP motif (17; see also Swartz (18)).

The consistency of the constraints by Webster et al. (17) with the available x-ray structures has not yet been tested in a molecular modeling study. Such study is necessary, in particular, because the current interpretation of the Cd^{2+}-binding experiments involves certain ambiguity. On one hand, the fact that Cd^{2+} blocks the double mutant Val-474-Cys/Val-476-Cys suggests that the pore lumen should be as small as the diameter of a Cd^{2+} ion. On the other hand, the open pore should be wide enough to accommodate flexible quaternary ammonium blockers and permeate hydrated K^+ ions. To compromise these observations, Webster et al. (17) proposed that the width of the open pore may vary from ~3 to ~8–9 Å.

The upper estimate of the pore dimension proposed by Webster et al. (17) is deduced from the size of flexible ligands that block the channel. The interpretation of data on flexible drugs binding in terms of the pore dimensions requires analysis of conformation-activity relationships (19). More rigid open-channel blockers may provide direct estimates of the minimal width of the cytoplasmic pore entrance. One such blocker is correolide, a nortriterpene alkaloid isolated from the Costa Rican tree *Spachea correa* (20). Correolide prevents T-cell activation and attenuates immune responses by selectively blocking open (or C-type-inactivated) Kv1.3 channels in T cells (21). Besides Kv1.3, the drug blocks other members of the *Shaker* subfamily (22). Correolide interacts with several residues in the inner helix, suggesting that the binding site is located inside the pore (23). Correolide has a semirigid hexacyclic core, which makes the drug an ideal candidate to probe the dimensions of the open *Shaker* channel.

In this work we use molecular modeling to explore whether available experimental data on the dimensions of the *Shaker* open pore are consistent with available crystallographic structures of bacterial K^+ channels. We first calculate the cross-sectional dimensions of correolide and demonstrate that it matches the width of KvAP at the level of the cytoplasmic entrance to the open pore. We further build KcsA-, MthK-, and KvAP-based models of the *Shaker* mutant Val-476-Cys and apply distance constraints Cys-476—Cd^{2+}—His-486 to impose the locked-open conformations. The KvAP-based model readily accommodates the constraints, whereas KcsA- and MthK-based models seem inconsistent with the Cd^{2+}-binding data. Finally, we create the KvAP-based model of the double mutant Val-474-Cys/Val-476-Cys in the locked-open conformation and simulate Cd^{2+} block at the level of engineered Cys-474. The model readily accommodates two but not one Cd^{2+} ion at this site. Our study shows that experimental constraints of Webster et al. (17) are consistent with the x-ray structure of KvAP. These data imply that the geometry of the pore region of the open *Shaker* is similar to that of KvAP.

METHODS

Energy calculations were performed using the Monte-Carlo-minimization (MCM) method (24), AMBER force field (25), and the ZMM program (www.zmmsoft.com) as described elsewhere (26). The hydration energy was calculated by the implicit-solvent method (27). Ionizable residues were kept in their neutral forms, except for the Cd^{2+}-bound cysteines, which were modeled in the deprotonated forms. The energy minimizations were performed in the space of generalized coordinates, which included torsional angles, bond angles of ligands, Cartesian coordinates of ions, Cartesian coordinates of root atoms of free molecules, and Euler angles of local coordinate systems at the root atoms. The homology models of the *Shaker* channel and its Val-474-Cys and Val-476-Cys mutants were built using the alignment shown in Table 1. The starting KcsA-, MthK-, and KvAP-based models of the *Shaker* channel and its Val-476-Cys mutants were built and MC-minimized using the approach described elsewhere (26).

TABLE 1 Alignment of K^+ channels

Outer helices					
		1	11	21	31
KcsA	14	KLLLGRHGSA	LHWRAAGAAT	VLLVIVLLAG	SYLAVLAE
MthK	5	IEIIRKHLPR	VLKVPATRIL	LLVLAVIIYG	TAGFHFIE
KvAP	135	SKFLSAIADA	ADKIRFYHLF	GAVMLTVLYG	AFAIYIVE
Shaker	381	GLQILGRTLK	ASMRELGLLI	FFLFIGVVLF	SSAVYFAE
Inner helices					
		1	11	21	31
KcsA	86	LWGRLVAVVV	MVAGITSFGL	VTAALATWFV	GREQ
MthK	70	PLGMYFTVTL	IVLGIGTFAV	AVERLLEFLI	NREQ
KvAP	207	PIGKVIGIAV	MLTGISALTL	LIGTVSNMFQ	KILV
Shaker	453	VWGKIVGSLC	**A**IAG**V**LTI**A**L	**PVP**VIVSNFN	YFYH

Correolide-sensing residues in the inner helices of Kv1.3 (23) are in bold print.

Determining dimensions of *Shaker* channel blockers

The dimensions of correolide and tetrabutylammonium were determined by computing plots of MC-minimized energy of the drug pulled through variable-diameter rings of methane molecules. The epoxy oxygen of correolide was constrained to a movable plain P_O, which is parallel to the ring plane. Plane P_O was translated with a step of 0.5 Å, and at each step the energy was MC-minimized. The translational position of correolide at the plots corresponds to the displacement of plane P_O from the ring plane. To prevent the flip-flop of correolide during MCMs, an atom in the seven-membered ring of correolide was constrained not to occur ahead of plane P_O.

Modeling the Cd^{2+}-bound *Shaker* channel

The locked-open conformations of the channel were built to satisfy distance constraints between Cys-476 and His-486 residues (17). In the starting KcsA-, MthK-, and KvAP-based models, the distances between Cys-476 and His-486 residues were too large to form Cd^{2+} bridges described by Webster et al. (17). The lengths of coordinating bonds S—Cd^{2+} and N—Cd^{2+} are known from the crystal structures of small molecules with Cd^{2+}. Applying the lengths of the coordinating bonds as fixed distance constraints Cys-476_S^{γ}—Cd^{2+}—$N^{\varepsilon 2}$_His-486 to the x-ray based models of the *Shaker* caused abrupt conformational changes and bad contacts, which were difficult to relax in a reasonable computational time. Therefore, each x-ray-based model of the *Shaker* was modified in a series of MCM trajectories with fixed distance constraints Cd^{2+}—S^{γ}_Cys-476 and variable, gradually diminishing constraints Cd^{2+}—$N^{\varepsilon 2}$_His-486 (26). The starting values of the latter constraints were calculated in the MCM trajectory in which the protein backbones were kept rigid, whereas side-chain torsions and positions of Cd^{2+} ions were varied to minimize mismatch with the experimental lengths of coordinating bonds N—Cd^{2+}. In the subsequent series of MCM trajectories, the variable distance constraints were diminished with a step of 0.5 Å. At each step, the energy was MC-minimized starting from the optimal structure found at the previous step.

In the constraints-driven MCM trajectories, the alpha carbons in the P-loops as well as in the extracellular halves of the inner and outer helices were constrained to the respective crystallographic positions using pins, flat-bottom energy functions with a bottom width of 1 Å. The secondary structure of the C-terminal parts of the inner helices (Ser-479 through His-486) was preserved by constraining α-helical H-bonds between CO and NH groups. MCM trajectories were terminated when the last 2000 consecutive energy minimizations did not decrease the lowest energy found. At the last stage of simulating the locked-open conformations of the *Shaker* channel, all constraints were removed and an additional MCM trajectory was run. This protocol ensured smooth conformational changes that yielded a compromise between the starting x-ray-based structure of the *Shaker* channel and the experimental S—Cd^{2+} and N—Cd^{2+} constraints. The same methodology was also used to simulate the Cd^{2+} block of the locked-open *Shaker* channel.

Simulating Cd^{2+} ions

Classical force-field parameters for Cd^{2+} do not reproduce experimental geometry of Cd^{2+}-Cys complexes (28) and quantum-chemical methods are impractical for large systems. Therefore, we simulated Cd^{2+} using AMBER parameters for Mg^{2+}. This approximation had little effect on calculations in which bonds with Cd^{2+} were constrained. In the nonconstrained trajectories, the strong electrostatic attraction of the divalent cation to electronegative atoms influenced the formation of coordinating bonds. Too-close coordination of the divalent cation with the electronegative atoms was precluded by flat-bottom penalty functions with no upper-distance limit and lower-distance limits of 2.65, 2.3, and 2.47 Å, which are seen in the x-ray structures of Cd^{2+} coordinated to sulfur (29), nitrogen (30), and oxygen (29), respectively. Subsequent removal of the flat-bottom penalty functions and additional energy minimizations did not noticeably change the complexes found. Test calculations with Ca^{2+} and Zn^{2+} in place of Cd^{2+} resulted in practically the same conformations as with Mg^{2+}.

RESULTS AND DISCUSSION

Dimensions of the *Shaker* blockers

The dimensions of semirigid open-channel blockers may provide direct estimates of the minimal width of the cytoplasmic pore entrance. Correolide has a flattened-ellipsoid shape with a hexacyclic core decorated with six acetoxy groups (Fig. 1). The maximal length of correolide, measured between oxygen atoms at the ellipsoid poles, is 13.6 Å. The dimensions of correolide in directions normal to the long axis depend on orientations of acetoxy groups. To determine these dimensions, we created circular constructs of 14–18 methane molecules of variable inner diameter $d_i = d_c - 4$ Å, where d_c is the diameter of the circle drawn via centers of carbon atoms and 4 Å is an approximate van der Waals diameter of methane. The number of methane molecules increased with the ring diameter to sustain the distance of ~3 Å between adjacent carbons. The drug was pulled through the rings with a step of 0.5 Å and at each position the energy was optimized using the MCM protocol (Fig. 2, *A* and *B*). Large energy barriers were obtained for correolide pulled through rings with $d_i < 10$ Å (Fig. 2 *A*). The 10-Å ring is also smaller than the minimal-profile projection of correolide in the energetically optimal conformation (Fig. 3 *A*). However, the drug can pass through this ring by adopting more compact conformations. (A pore entrance in an open channel may experience rare fluctuations during which the cross-sectional dimensions could increase. However, short-lived fluctuations are unlikely to contribute to the high-affinity binding of bulky drugs as discussed in a later section.) Analogous calculations show that tetrabutylammonium could pass through a ring as small as 7–8 Å (Fig. 2, *C* and *D*).

Pro-475 residues form the narrowest level at the cytoplasmic entrance to the pore of the KvAP-based model of the *Shaker* channel (Fig. 3, *B* and *C*). The distance of 14.4 Å between diagonally opposed atoms C^{γ}_Pro-475 remarkably matches the ring of $d_c = 14$ Å ($d_i = 10$ Å). Several correolide-sensing residues line the pore (23), suggesting

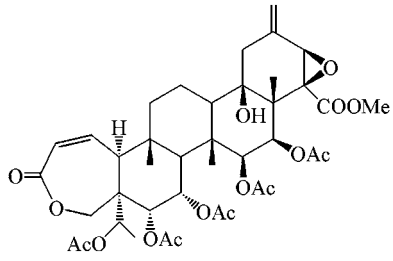

FIGURE 1 Structure of correolide.

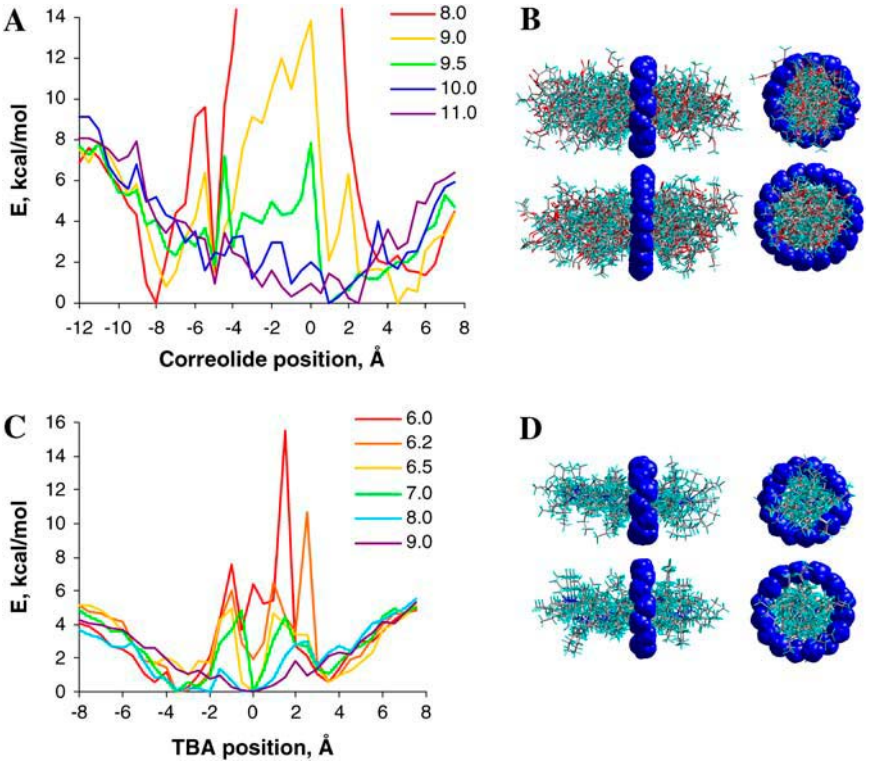

FIGURE 2 Dimensions of *Shaker* channel intracellular blockers. (*A*) Plots of MC-minimized energy of correolide pulled via the variable-diameter rings of methane molecules. The zero position corresponds to the epoxy group of correolide in the plane of the ring. The energy barrier increases sharply as the diameter decreases from 10 to 9.5 Å. (*B*) The superposition of MC-minimized structures of correolide pulled through the rings with inner diameter d_i of 8 and 10 Å. Large deformations of correolide in the smaller ring explain the high energy barrier shown in *A*. MCM caused some methane molecules of the smaller ring to violate in-plane constraints to avoid strong repulsions with their neighbors. (*C*) Plots of MC-minimized energy of tetrabutylammonium pulled via the variable-diameter rings of methane molecules. The zero position corresponds to the nitrogen atom in the plane of the ring. The barrier increases sharply as the diameter decreases from 6.5 to 6 Å. (*D*) The superposition of MC-minimized structures of tetrabutylammonium pulled through the rings inner diameter d_i of 6 and 8 Å.

that correolide binds between the entrance and the selectivity filter. Fig. 3 *B* shows Pro-475 residues aligned with the ring of $d_i = 10$ Å. The latter embraces correolide molecules in which the epoxy oxygen is displaced 0–8 Å from the ring plane. In the topmost position, the drug's pole would reach the selectivity filter, whereas part of the drug would remain outside the entrance (Fig. 3 *B*), suggesting that the entrance narrower than 10 Å would not accommodate correolide. In T lymphocytes, the development of the K^+ current block by correolide is slow (21), but intracellular application results in a faster block (31). In the KvAP-based model, the correolide-binding site has a cylindrical shape (Fig. 3 *B*). The energy barrier for a drug entering such a site should inversely correlate with the binding energy. Correolide binds with a high affinity (21), suggesting that the native conformation of the *Shaker* open pore is wide enough to accommodate the drug.

Locked-open conformations of the *Shaker* channel

To explore the consistency of the data on Cd^{2+} locking the open *Shaker* with crystallographic structures of bacterial K^+ channels, we created KvAP-, MthK-, and KcsA-based models of the *Shaker* mutant Val-476-Cys. When α-carbons were constrained (pinned) to the corresponding x-ray templates, the models failed to form Cys-476_S^{γ}—Cd^{2+}—$N^{\varepsilon 2}$_His-486 bridges, indicating the necessity of backbone deformations. Current theories suggest that such deformations would occur at the gating-hinge Gly-467 (2) or the PVP motif (17) or at both. To test these theories, we removed all pins at the intracellular half of the channel and ran series of consecutive MCM trajectories, in which distance constraints Cys-476_S^{γ}—Cd^{2+}—$N^{\varepsilon 2}$_His-486 were gradually introduced to yield locked-open conformations.

The KvAP-based model converged to the energetically preferable structure, which was similar to the starting x-ray structure (Fig. 4; Table 2). In the KvAP-based model of the locked-open *Shaker*, each Cd^{2+} ion coordinates the side chains of Cys-476 and His-486 in the inner helices and Glu-395 in the outer helix (Fig. 5, *A* and *B*). Interestingly, no constraints were imposed between Cd^{2+} and Glu-395, which was kept neutral in the model. Despite that, the coordinating bonds Cd^{2+}—Glu-395 were formed, exemplifying the notion that Cys, His, and Asp form Cd^{2+}-binding sites in proteins (32,33). This finding is experimentally testable. If proven, it would serve as a strong argument in favor of the proposed alignment of the outer helices (Table 1). Both electrostatic and van der Waals interactions are more favorable in the locked-open conformation than in the starting conformation. Superimposing the 10-Å ring of methane molecules with the locked-open KvAP-based model of *Shaker* shows a remarkable match in the pore diameter, which is minimally required to accommodate correolide (Fig. 3 *C*).

The KcsA-based model underwent small deformations to accommodate Cys-476_S^{γ}—Cd^{2+}—$N^{\varepsilon 2}$_His-486 constraints, but at the expense of a large energy increase. The resultant model cannot be categorized as the locked-open

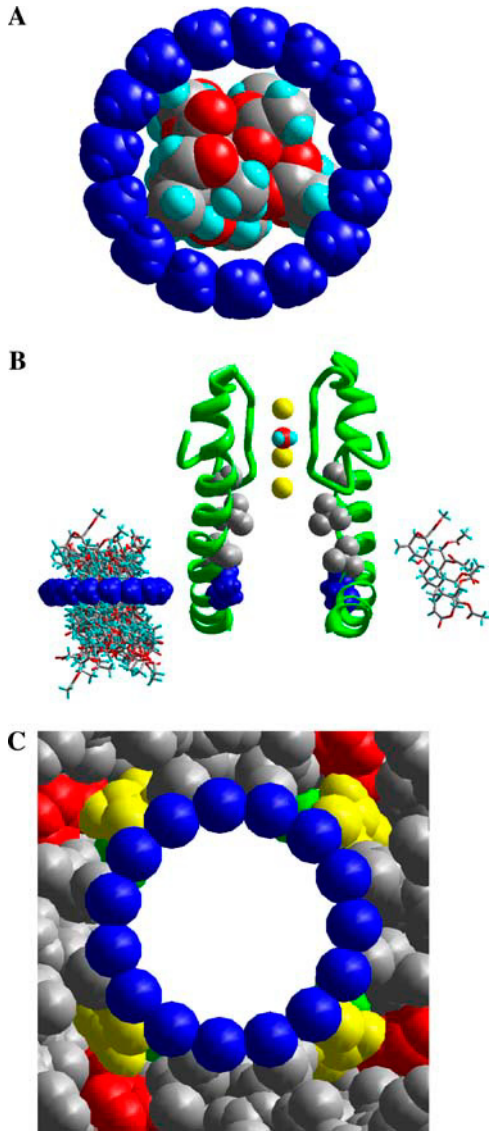

FIGURE 3 The 10-Å ring of methane molecules versus correolide and KvAP-based model of the *Shaker* channel. (*A*) Space-filled model of correolide viewed via the ring. (*B*) The side view of the *Shaker* model. The inner helices in two opposite domains are shown as ribbons. C-terminal parts of the pore helices and the selectivity-filter region are shown as rods. Correolide-sensing residues Ala-463, Val-467, Ala-471, Val-474, and Pro-475 are space-filled. Blue-colored Pro-475 at the cytoplasmic entrance is aligned with the 10-Å ring embracing correolide molecules in positions 0 through 8 Å from the ring plane (*left*). In the latter position (*right*), correolide would occur between the selectivity filter and the cytoplasmic entrance to the pore, which should be at least 10 Å wide to enable high-affinity binding of the drug. (*C*) Space-filled model of the KvAP-based model of the *Shaker* channel viewed via the 10-Å ring. Pro-473, Val-474, and Pro-475 are colored red, yellow, and green, respectively. Hydrogen atoms are not shown. Note a perfect match in the dimensions of the ring and the cytoplasmic entrance to the pore.

channel, since the pore remained in the closed conformation (Fig. 4). MCM trajectories of the MthK-based model with the locking-open constraints converged to an energetically favorable conformation, but it was significantly different from the starting structure (Fig. 4; Table 2). Unexpectedly and importantly, the final locked-open conformation occurred rather similar to the KvAP-based locked-open conformation (Fig. 5, *C* and *D*; Table 2).

Thus, among the three x-ray structures tested, only the KvAP-based model readily accommodated the Cys-476_S^{γ}—Cd^{2+}—$N^{\varepsilon 2}$_His-486 constraints, producing a locked-open conformation. The opening of the Ca^{2+}-gated channel MthK is driven by the inner helices linked to the cytoplasmic Ca^{2+}-binding domains. The opening of the voltage-gated channel KvAP is driven by the outer helices linked to the voltage-sensing domains. The different mechanisms of activation may account for the different pore geometry observed in the crystal structures of these channels. The consistency of the KvAP-based model of the *Shaker* channel with Cd^{2+}- and correolide-binding experiments suggests that the pore region of KvAP retains a nativelike conformation in the crystal.

Conformational changes at the PVP motif

In all the locked-open models, the inner helices did not kink at the PVP motif, but bent at residues N-terminal to it. This result agrees with the conclusion from the statistical analysis of crystallographic structures of proline-containing transmembrane helices that kinks occur not at prolines per se, but at residues three to four positions N-terminal to the prolines (34). In the *Shaker* channel, Pro-473 and Pro-475 deprive backbone carbonyls between Thr-468 and Leu-472 of H-bond donors, thus increasing the flexibility of residues C-terminal to Gly-467, which aligns with the gating hinge in prokaryotic K^+ channels. This region also undergoes the largest conformational changes during in silico activation of KcsA by lateral forces applied to the C-termini of inner helices (26). Our calculations show that Cd^{2+} binding causes conformational changes between the conserved Gly and the PVP motif (Fig. 6), but the latter does not show substantial kinks.

Another argument in favor of a sharp bend at the *Shaker* PVP motif was raised by del Camino et al. (15), who studied how the open-channel blockers protect engineered cysteines in the inner helices from the chemical modification by methanethiosulfonate reagents. The authors demonstrated, in particular, that tetrabutylammonium protects engineered cysteines in positions 470, 474, and 478, but not in positions 476, 482, and 483. Despite the fact that our model does not include the kink at the PVP motif, it agrees with the experimental observations of del Camino et al. (15), as well as with their prediction that side chains in positions 470, 474, and 478 face the pore, position 476 faces away from the pore, and positions 482 and 483 are far from the pore axis.

Calculations of the full-fledged models of the *Shaker* channel were performed taking advantage of the fourfold symmetry of the channel. As a control, we ran a series of constrained MCMs of the KvAP-based inner-helix bundle without employing the symmetry operations. The search yielded a slightly asymmetric locked-open structure (Fig. 6,

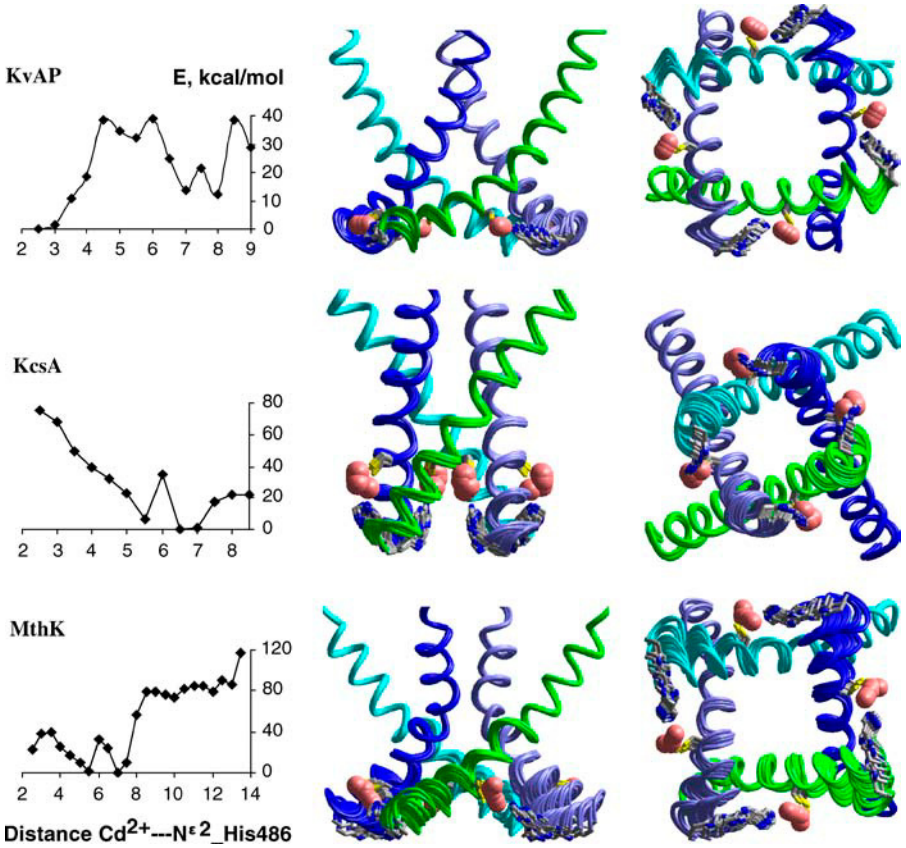

FIGURE 4 Convergence of the *Shaker* models from the x-ray-based starting structures to conformations with coordinating bonds Cys-476_S^{γ}—Cd^{2+}—$N^{\varepsilon 2}$_His-486. Cd^{2+} ions were constrained to S^{γ}_Cys-476 at the distance of 2.65 Å. Distance constraints Cd^{2+}—$N^{\varepsilon 2}$_His-486 were decreased with a step 0.5 Å from the starting values found in the x-ray-based structures. At each step, the energy was MC-minimized until the distances of ~2.3 Å were achieved. In the plots of MC-minimized energy against the imposed distance Cd^{2+}—$N^{\varepsilon 2}$_His-486, the energy is shown relative to the lowest-energy structure found. The locked-open conformations are more preferable energetically than the starting KvAP- and MthK-based structures. KcsA-based conformation with coordinating bonds Cys-476_S^{γ}—Cd^{2+}—$N^{\varepsilon 2}$_His-486 has higher energy than the starting structure. Superposed MC-minimized structures are at the right of the respective energy plots. In the side and cytoplasmic views, only the inner helices are shown for clarity. Cys and His are shown as sticks and Cd^{2+} ions as magenta spheres. Locking open the KvAP-based structure is energetically preferable and requires minimal structural deformations.

A and *B*), in which disposition of the inner helices is very similar to that in the symmetric model (Fig. 5, *A* and *B*). The comparison of torsions in the starting and locked-open structures shows that major changes occur at Ile-470, one helical turn upstream to the PVP motif. (Fig. 6, *C* and *D*). To increase the probability of backbone deformations at the PVP motif, additional simulations of the locked-open conformations were performed with elastic bond angles varied in the PVP residues. Calculations with rigid and elastic bond angles at the PVP motif gave similar results.

Thus, the KvAP-based model of the *Shaker* channel is consistent with experimental observations that were interpreted in favor of a sharp kink at the PVP motif. However, instead of a sharp kink, the model shows a smooth bend of the inner helices between the conserved Gly and the PVP motif. If the PVP motif does not cause a kink, why is it conserved in *Shaker* channels? A possible reason is an increased flexibility of the inner helices, which may be important for the gating of the *Shaker* channel (35) and possibly for its regulation.

TABLE 2 Comparison of the *Shaker* channel models

Compared models	RMSD (Å) of C^{α} atoms in the inner-helix residues*				
	1–3	14–20	21–24	25–34	1–34
X-ray KvAP versus locked-open KvAP-based	1.06	1.21	1.40	4.19	2.48
X-ray KcsA versus constrained KcsA-based†	0.95	2.03	2.44	3.95	2.55
X-ray MthK versus locked-open MthK-based	1.17	1.24	2.01	4.84‡	3.39‡
X-ray MthK versus x-ray KvAP	1.86	2.54	3.53	6.20‡	3.37‡
Locked-open MthK-based versus locked-open KvAP-based	2.77	2.58	2.52	2.55‡	2.65‡

*Relative residue numbers, see Table 1. RMSD, root mean-square deviation.
†MCM with constraints Cys-476—Cd^{2+}—His-486 did not produce the open conformation of the channel.
‡The inner helix ends at residue 29, which is the last residue in the MthK x-ray structure.

Simulating the Cd^{2+} block of the locked-open *Shaker* channel

Block by a single cadmium ion

The observation that Cd^{2+} blocks the locked-open *Shaker* double mutant Val-474-Cys/Val-476-Cys by coordinating Cys-474 implies that the pore lumen at the level of S^{γ}_Cys-474 could be as small as the diameter of a Cd^{2+} ion (17). A much wider lumen is needed to accommodate hydrated K^{+} and certain blockers (17), implying that Cd^{2+} block would

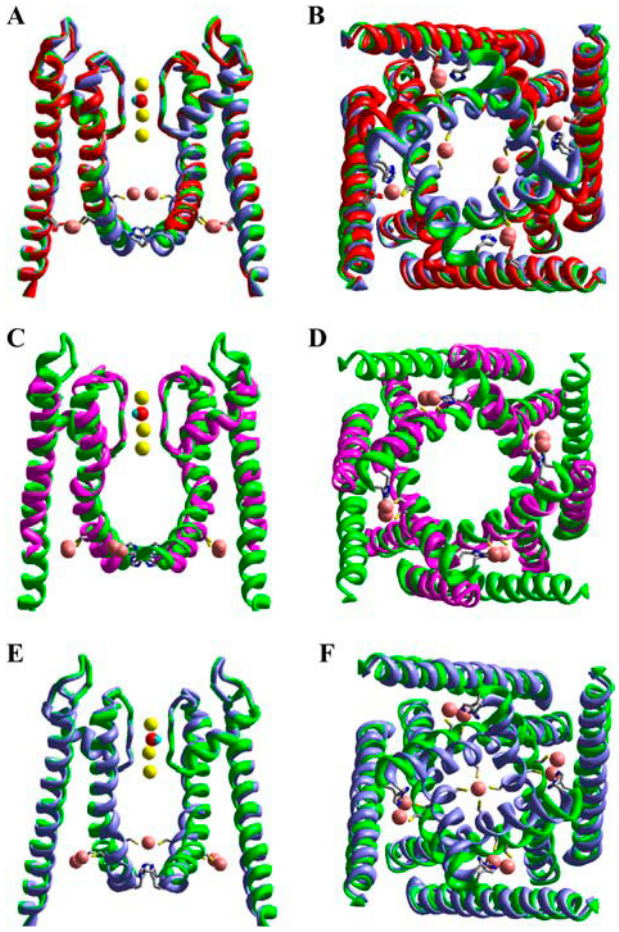

FIGURE 5 KvAP-based models of the *Shaker* channel. (*A* and *B*) Side and cytoplasmic views of the superposition of the x-ray based structure (*red*), locked-open mutant Val-476-Cys (*green*), and locked-open mutant Val-474-Cys/Val-476-Cys (*violet*) blocked by two Cd^{2+} ions. The side chains of Glu-395, Cys-476, and His-486 are shown as sticks, Cd^{2+} ions as magenta spheres, and K^+ ions as yellow spheres. The involvement of Glu-395 in the Cd^{2+} coordination sphere was an unexpected result of MCM. The coordination occurred despite Glu-395 was not ionized in the model. In the cell, negative charges at Glu-395 and Cys-474 would facilitate Cd^{2+} binding. (*C* and *D*) The superposition of the locked-open conformations obtained from KvAP (*green*) and MthK (*magenta*) starting structures. The conformations are similar despite starting structures being essentially different, especially at the C-termini (Table 2). For clarity, only two opposed domains are shown in the side views and only inner and outer helices are shown in cytoplasmic views. (*E* and *F*) The superposition of the locked-open model (*green*) and the locked-open model blocked by a single Cd^{2+} ion (*violet*). Constraining a single Cd^{2+} ion to four Cys-474 residues caused large conformational deformations, which are inconsistent with the experimentally observed easiness of the Cd^{2+} block of the locked-open channel.

cause essential conformational changes of the locked-open *Shaker*. To evaluate these changes, we built the KvAP-based model of the *Shaker* double mutant, retained the eight locking-open constraints with the four Cd^{2+} ions, and imposed constraints between the fifth Cd^{2+} ion and four Cys-474 residues. The constrained MCM trajectories were run to yield the Cd^{2+}-blocked locked-open conformation. The KvAP-based model blocked by a single Cd^{2+} deviated significantly from the starting locked-open conformation (Fig. 5, *C* and *D*).

The variable diameter of the locked-open *Shaker* was proposed to explain different dimensions of organic and inorganic blockers acting at the same region of the open pore (17). However, large deformations that would be caused by the Cd^{2+} coordination to three or four Cys-474 residues are inconsistent with the observed easiness with which the *Shaker* double mutant assumes a Cd^{2+}-blocked conformation from the locked-open state (17). The problem arises from the assumption that at least three Cys-474 residues should coordinate Cd^{2+} simultaneously (17). This assumption is backed by the observation that channels with four Cys-474 bind Cd^{2+} irreversibly, whereas channels with two Cys-474 bind Cd^{2+} reversibly (36). It should be noted that the channels with two Cys-474 were expressed as tandems of two dimers with a 474 mutation only in the first protomer (36). In such tandems, Cys474 are at the opposite inner helices and cannot coordinate Cd^{2+} simultaneously in the open channel.

Block by two cadmium ions

In an alternative model, two pairs of the negatively charged residues would chelate two divalent cations. Such a pattern was proposed in the selectivity-filter models of Ca^{2+} channels (10, 37) and is seen in the x-ray structure of a Ca^{2+} pump (38). MCM of the locked-open KvAP-based model of *Shaker* blocked by two Cd^{2+} ions at Cys-474 residues caused only small backbone deformations (Fig. 5, *A* and *B*). In terms of the coordination number, the model with two Cd^{2+} ions seems less preferable than the model, in which Cd^{2+} is tetracoordinated by four Cys-474 residues. However, the coordination stereochemistry of Cd^{2+} is known to be unusually variable, including coordination numbers from 2 to 8 (39). Coordination of Cd^{2+} by two Cys residues was demonstrated in the *Shaker* channel (17). Another advantage of the model blocked by two Cd^{2+} ions is an electrostatic balance between positive charges at Cd^{2+} ions and negative charges at Cys-474 residues.

Two Cd^{2+} ions chelated by Cys-474 residues do not physically occlude the pore, raising the question about the mechanism of the K^+ current block. To address this question, we estimated the energy barrier of a hydrated K^+ ion pulled via the *Shaker* double mutant Val-476-Cys/Val-474-Cys using methodology described elsewhere (40). The hydration shell of the K^+ ion included eight water molecules. The solvation shell of each Cd^{2+} ion included five water molecules in addition to two sulfur atoms from Cys-474 residues. The oxygen atom of each water molecule was constrained to the respective cation via a distance penalty function that prevented oxygen-metal separation by >3 Å. These constraints were necessary because the model did not include water molecules beyond the first hydration shells, which in a real system would substitute a water molecule abandoning a cation. We did not consider an unlikely

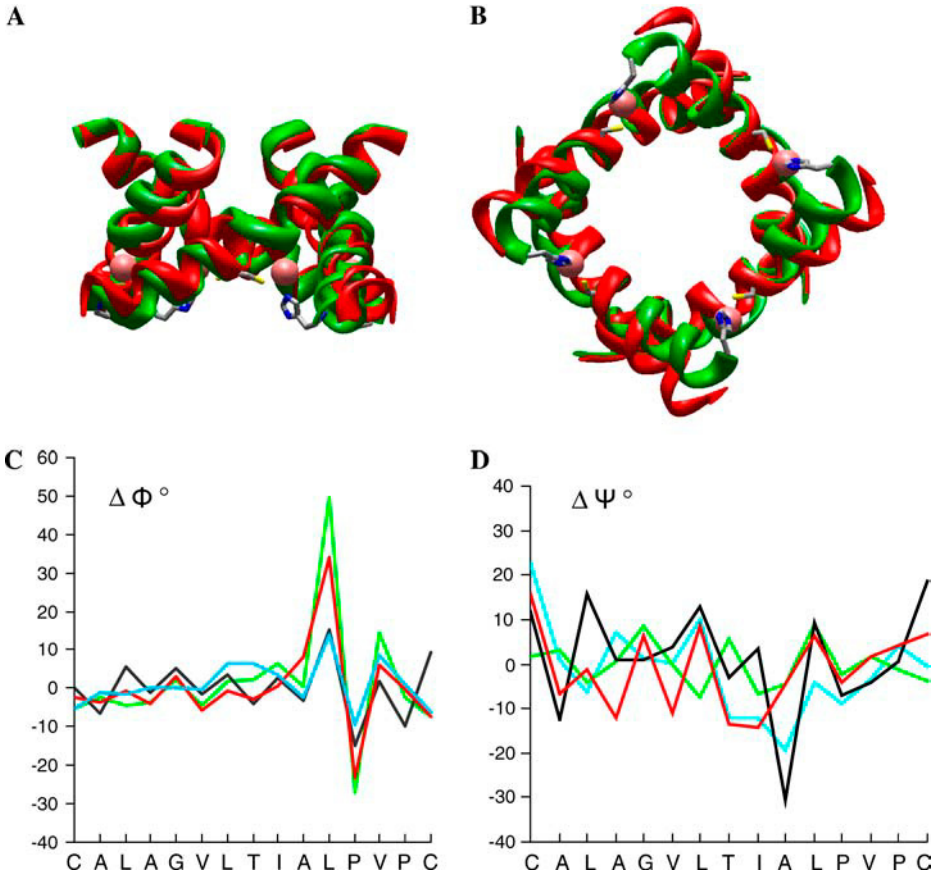

FIGURE 6 KvAP-based model of the *Shaker* inner-helices bundle obtained by MCM without using the advantage of the channel fourfold symmetry. (*A* and *B*) Side and cytoplasmic views of superposition of KvAP x-ray structure (*red*) and locked-open *Shaker* mutant Val-476-Cys (*green*). The side chains of Cys-476 and His-486 are shown as sticks. K^+ and Cd^{2+} ions are shown as spheres. The inner helices bend smoothly at residues N-terminal to the PVP motif. (*C* and *D*) Changes of backbone torsions in four subunits observed during the simulated locking of the open channel starting from the KvAP-based conformation. Largest changes of Φ are at Leu-472 and Pro-473 and moderate changes are in segments both N- and C-terminal to the PVP motif. Largest changes of Ψ are at Ala-471, whose backbone oxygen lacks the helical H-bond. Changes at Ile-478 through His-486 are not shown because torsions were restrained in alpha-helical conformation. Changes at Leu-461 are not shown because this residue was constrained at conformation seen in KvAP.

scenario of sharing a water molecule between the first hydration shells of two closely spaced cations.

The hydrated K^+ ion was constrained to a plane normal to the pore axis. The plane was translated with a step of 0.5 Å and at each step the energy of the entire system was MC-minimized. The calculations predicted that the hydrated K^+ pulled from the cytoplasm through the level of Cys-474 with two Cd^{2+} ions would encounter an energy barrier of 36.2 kcal/mol (Fig. 7 *A*). The barrier has two major components: 1), electrostatic energy of K^+, whose repulsion from Cd^{2+} ions is stronger than the attraction to ionized Cys-474 residues; and 2), energy of the K^+ hydration shell in which some hydrogen atoms would occur too close to the Cd^{2+} ions (Fig. 7 *B*). These simple calculations suggest that K^+ permeation via the *Shaker* double mutant blocked by two Cd^{2+} ions is hardly possible. Thus, the KvAP-based model of the *Shaker* channel is consistent with the distance constraints known from the action of Cd^{2+} ions and organic blockers. Our results indicate that the pore region is structurally conserved between prokaryotic and eukaryotic K^+ channels.

Sensitivity of results to the chosen computational methodology

Experimental data on the binding of correolide and Cd^{2+} ions to *Shaker* channels provide seemingly conflicting constraints on the open pore geometry. Cd^{2+}-binding constraints are not consistent with available x-ray structures, and their interpretation requires the modeling of the backbone deformations. For this goal, we applied the methodology of MCM in the space of generalized coordinates, which was recently used for the simulations of large-scale conformational transitions in KcsA (26). Three x-ray structures of K^+ channels were used as the starting points. The KvAP structure underwent minimal conformational deformations to accommodate the distance constraints from experiments on the *Shaker* Val-476-Cys mutant locked open by Cd^{2+} ions, but the pore remained wide enough to accommodate a large molecule of correolide.

Results of molecular simulations are not always confirmed by subsequent experiments. Therefore, the sensitivity of our results to the chosen computational methodology should be discussed. Pulling correolide through the rings of methane molecules predicts energy barriers that rule out correolide binding in rings <10 Å. The barriers are determined by repulsive forces, which are similar in different force fields. Entropy was ignored, but its inclusion would increase rather than decrease the free energy barrier at the critical diameter of the ring, which is matched by one of many possible conformations of correolide. Our simulations of the *Shaker* channel in different states depend on the applied constraints, starting geometry, energy optimization method, and force

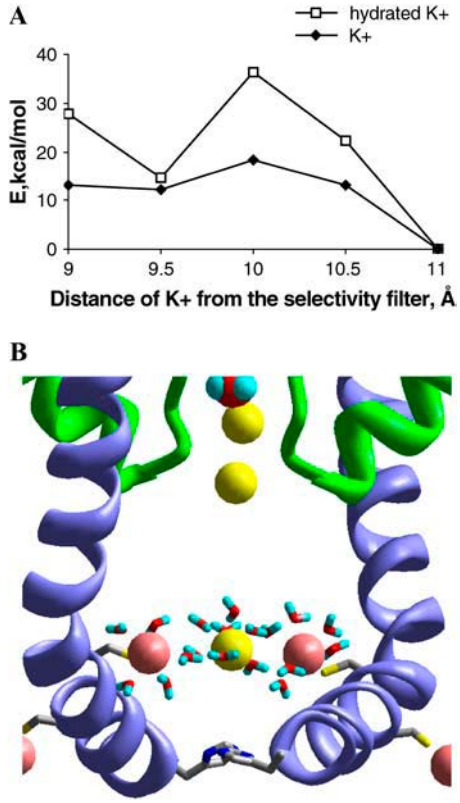

FIGURE 7 (*A*) Energy of a K^+ ion (♦) and the same ion with the first hydration shell comprising eight water molecules (□) pulled via the *Shaker* locked-open double mutant Val-474-Cys/Val-476-Cys blocked by two Cd^{2+} ions. The pulling was accomplished by constraining K^+ to the plane, which was translated normally to the pore axis. The abscissa shows the distance (d) between the plane and the K^+ ion bound to Thr residues in the selectivity-filter sequence TVGYG. The energy values are partitioned from the structures MC-minimized at each position of the K^+-constraining plane. The energies are given relative to the point $d = 11$ Å. Note that at position $d = 10$ Å, K^+ contributes ~50% to the energy barrier, and eight water molecules contribute the remaining ~50%. (*B*) MC-minimized structure with hydrated K^+ constrained at the level of $d = 10$ Å. In addition to electrostatic repulsion between the closely spaced cations, the system is destabilized by the unfavorable orientation of water molecules, some of which cannot avoid exposure of their hydrogen atoms to Cd^{2+} ions.

fields. The constraints used are defined in experiments. Three different x-ray structures of K^+ channels were tested as starting approximations and the KvAP structure was found to be most consistent with the constraints. The MCM protocol is a highly efficient method of nonlocal conformational search (24). Force-field parameters can be questioned in any computational work. However, these parameters are less critical in our study, which does not explore relative probabilities of various structures, but addresses consistency of the available x-ray structures of K^+ channels with experiments on Cd^{2+} binding to the *Shaker* mutants.

CONCLUSIONS

X-ray structures of bacterial K^+ channels are widely used for homology modeling of eukaryotic channels. However, the reliability of the models is questioned by controversial interpretations of experiments addressing structural similarity between eukaryotic and prokaryotic K^+ channels. On one hand, substituting the prokaryotic pore into the *Shaker* channel suggests conservation of the pore domain between the channels (14). On the other hand, experiments on Cd^{2+} action to the *Shaker* channel with engineered cysteines (15–17) imply structural differences between eukaryotic and prokaryotic K^+ channels.

In this work, we have shown that the distance constraints derived from the experiments on locking open the *Shaker* mutants (17), as well as the seemingly paradoxical ability of large correolide (23) and small Cd^{2+} ions (17) to block the open *Shaker* in the same region of the pore, are consistent with the KvAP structure. These data imply a structural conservation between the pore regions in prokaryotic and eukaryotic voltage-gated potassium channels.

A possibility that the antibody in the KvAP crystal structure distorts the mutual disposition of the voltage-sensor and pore domains is disputed (41,42). Distortion of the pore domain per se, which is stabilized by multiple intradomain contacts and does not form direct contacts with the antibody, seems less likely. Our finding that the KvAP-based structure is consistent with the distance constraints derived from cadmium- and ligand-binding experiments on the open *Shaker* channel can be explained in two ways. One possibility could be that both antibody binding to KvAP and Cd^{2+} binding to the *Shaker* mutant induce similar distortions in the native conformations of the proteins. However, the fact that the KvAP-like structure was obtained upon locking open the MthK-based starting conformation supports a more likely possibility that the KvAP pore domain retains the native conformation in the crystal.

We thank Daniel Yang and Denis Tikhonov for helpful discussions.

This work was supported by grants from the National Science and Engineering Research Council of Canada and Canadian Institutes of Health Research. B.S.Z. is a recipient of the Canadian Institutes of Health Research Senior Scientist award. Computations were performed, in part, using the Shared Hierarchical Academic Research Computing Network (SHARCNET) Supercomputer Center at McMaster University.

REFERENCES

1. Doyle, D. A., J. Morais Cabral, R. A. Pfuetzner, A. Kuo, J. M. Gulbis, S. L. Cohen, B. T. Chait, and R. MacKinnon. 1998. The structure of the potassium channel: molecular basis of K^+ conduction and selectivity. *Science*. 280:69–77.
2. Jiang, Y., A. Lee, J. Chen, M. Cadene, B. T. Chait, and R. MacKinnon. 2002. Crystal structure and mechanism of a calcium-gated potassium channel. *Nature*. 417:515–522.
3. Jiang, Y., A. Lee, J. Chen, V. Ruta, M. Cadene, B. T. Chait, and R. MacKinnon. 2003. X-ray structure of a voltage-dependent K^+ channel. *Nature*. 423:33–41.
4. Jiang, Y., A. Lee, J. Chen, M. Cadene, B. T. Chait, and R. MacKinnon. 2002. The open pore conformation of potassium channels. *Nature*. 417:523–526.

5. Luzhkov, V. B., J. Nilsson, P. Arhem, and J. Aqvist. 2003. Computational modelling of the open-state Kv 1.5 ion channel block by bupivacaine. *Biochim. Biophys. Acta.* 1652:35–51.
6. Laine, M., M. A. Lin, J. P. A. Bannister, W. R. Silverman, A. F. Mock, B. Roux, and D. M. Papazian. 2003. Atomic proximity between S4 segment and pore domain in *Shaker* potassium channels. *Neuron.* 39:467–481.
7. Durell, S. R., I. H. Shrivastava, and H. R. Guy. 2004. Models of the structure and voltage-gating mechanism of the *Shaker* K^+ channel. *Biophys. J.* 87:2116–2130.
8. Lipkind, G. M., and H. A. Fozzard. 2000. KcsA crystal structure as framework for a molecular model of the Na^+ channel pore. *Biochemistry.* 39:8161–8170.
9. Tikhonov, D. B., and B. S. Zhorov. 2005. Modeling P-loops domain of sodium channel: homology with potassium channels and interaction with ligands. *Biophys. J.* 88:184–197.
10. Zhorov, B. S., E. Folkman, and V. S. Ananthanarayanan. 2001. Homology model of dihydropyridine receptor. Implications for L-type Ca^{2+} channel modulation by agonists and antagonists. *Arch. Biochem. Biophys.* 393:22–41.
11. Lipkind, G. M., and H. A. Fozzard. 2001. Modeling of the outer vestibule and selectivity filter of the L-type Ca^{2+} channel. *Biochemistry.* 40:6786–6794.
12. Tikhonov, D. B., J. R. Mellor, P. N. Usherwood, and L. G. Magazanik. 2002. Modeling of the pore domain of the GLUR1 channel: homology with K^+ channel and binding of channel blockers. *Biophys. J.* 82: 1884–1893.
13. Flynn, G. E., and W. N. Zagotta. 2003. A cysteine scan of the inner vestibule of cyclic nucleotide-gated channels reveals architecture and rearrangement of the pore. *J. Gen. Physiol.* 121:563–582.
14. Lu, Z., A. M. Klem, and Y. Ramu. 2001. Ion conduction pore is conserved among potassium channels. *Nature.* 413:809–813.
15. del Camino, D., M. Holmgren, Y. Liu, and G. Yellen. 2000. Blocker protection in the pore of a voltage-gated K^+ channel and its structural implications. *Nature.* 403:321–325.
16. Holmgren, M., K. S. Shin, and G. Yellen. 1998. The activation gate of a voltage-gated K^+ channel can be trapped in the open state by an intersubunit metal bridge. *Neuron.* 21:617–621.
17. Webster, S. M., D. del Camino, J. P. Dekker, and G. Yellen. 2004. Intracellular gate opening in *Shaker* K^+ channels defined by high-affinity metal bridges. *Nature.* 428:864–868.
18. Swartz, K. J. 2004. Opening the gate in potassium channels. *Nat. Struct. Mol. Biol.* 11:499–501.
19. Zhorov, B. S., N. B. Brovtsyna, V. E. Gmiro, N. Lukomskaya, S. E. Serdyuk, N. N. Potapyeva, L. G. Magazanik, D. E. Kurenniy, and V. I. Skok. 1991. Dimensions of the ion channel in neuronal nicotinic acetylcholine receptor as estimated from analysis of conformation-activity relationships of open-channel blocking drugs. *J. Membr. Biol.* 121:119–132.
20. Felix, J. P., R. M. Bugianesi, W. A. Schmalhofer, R. Borris, M. A. Goetz, O. D. Hensens, J. M. Bao, F. Kayser, W. H. Parsons, K. Rupprecht, M. L. Garcia, G. J. Kaczorowski, and R. S. Slaughter. 1999. Identification and biochemical characterization of a novel nortriterpene inhibitor of the human lymphocyte voltage-gated potassium channel, Kv1.3. *Biochemistry.* 38:4922–4930.
21. Koo, G. C., J. T. Blake, K. Shah, M. J. Staruch, F. Dumont, D. Wunderler, M. Sanchez, O. B. McManus, A. Sirotina-Meisher, P. Fischer, R. C. Boltz, M. A. Goetz, R. Baker, J. Bao, F. Kayser, K. M. Rupprecht, W. H. Parsons, X. C. Tong, I. E. Ita, J. Pivnichny, S. Vincent, P. Cunningham, D. Hora, Jr., W. Feeney, and G. Kaczorowski. 1999. Correolide and derivatives are novel immunosuppressants blocking the lymphocyte Kv1.3 potassium channels. *Cell. Immunol.* 197:99–107.
22. Hanner, M., W. A. Schmalhofer, B. Green, C. Bordallo, J. Liu, R. S. Slaughter, G. J. Kaczorowski, and M. L. Garcia. 1999. Binding of correolide to K(v)1 family potassium channels. Mapping the domains of high affinity interaction. *J. Biol. Chem.* 274:25237–25244.
23. Hanner, M., B. Green, Y. D. Gao, W. A. Schmalhofer, M. Matyskiela, D. J. Durand, J. P. Felix, A. R. Linde, C. Bordallo, G. J. Kaczorowski, M. Kohler, and M. L. Garcia. 2001. Binding of correolide to the K(v)1.3 potassium channel: characterization of the binding domain by site-directed mutagenesis. *Biochemistry.* 40:11687–11697.
24. Li, Z., and H. A. Scheraga. 1987. Monte Carlo-minimization approach to the multiple-minima problem in protein folding. *Proc. Natl. Acad. Sci. USA.* 84:6611–6615.
25. Weiner, S. J., P. A. Kollman, D. A. Case, U. C. Singh, C. Ghio, G. Alagona, S. Profeta, and P. Weiner. 1984. A new force field for molecular mechanical simulation of nucleic acids and proteins. *J. Am. Chem. Soc.* 106:765–784.
26. Tikhonov, D. B., and B. S. Zhorov. 2004. In silico activation of KcsA K^+ channel by lateral forces applied to the C-termini of inner helices. *Biophys. J.* 87:1526–1536.
27. Lazaridis, T., and M. Karplus. 1999. Effective energy function for proteins in solution. *Proteins.* 35:133–152.
28. Berweger, C. D., W. Thiel, and W. F. van Gunsteren. 2000. Molecular-dynamics simulation of the beta domain of metallothionein with a semi-empirical treatment of the metal core. *Proteins.* 41:299–315.
29. Stalhandske, C. M., C. I. Stalhandske, M. Sandstrom, and I. Persson. 1997. Crystal structure of N,N-dimethylthioformamide solvates of the divalent group 12 ions with linear coordination geometry for mercury(II), tetrahedral for zinc(II), and octahedral for cadmium(II). *Inorg. Chem.* 36:3167–3173.
30. Bebout, D. C., S. W. Stokes, and R. J. Butcher. 1999. Comparison of heteronuclear coupling constants for isostructural nitrogen coordination compounds of (111/113)Cd and (199)Hg. *Inorg. Chem.* 38: 1126–1133.
31. Wunderler, D., R. J. Leonard, M. Sanchez, and O. B. McManus. 1999. Block of lymphocyte potassium channels by correolide, a triterpene natural product. *Biophys. J.* 76:A186.
32. Paul-Soto, R., M. Zeppezauer, H. W. Adolph, M. Galleni, J. M. Frere, A. Carfi, O. Dideberg, J. Wouters, L. Hemmingsen, and R. Bauer. 1999. Preference of Cd(II) and Zn(II) for the two metal sites in Bacillus cereus beta-lactamase II: a perturbed angular correlation of gamma-rays spectroscopic study. *Biochemistry.* 38:16500–16506.
33. Heinz, U., R. Bauer, S. Wommer, W. Meyer-Klaucke, C. Papamichaels, J. Bateson, and H. W. Adolph. 2003. Coordination geometries of metal ions in d- or l–captopril-inhibited metallo-beta-lactamases. *J. Biol. Chem.* 278:20659–20666.
34. Cordes, F. S., J. N. Bright, and M. S. Sansom. 2002. Proline-induced distortions of transmembrane helices. *J. Mol. Biol.* 323: 951–960.
35. Labro, A. J., A. L. Raes, I. Bellens, N. Ottschytsch, and D. J. Snyders. 2003. Gating of *Shaker*-type channels requires the flexibility of S6 caused by prolines. *J. Biol. Chem.* 278:50724–50731.
36. Liu, Y., M. Holmgren, M. E. Jurman, and G. Yellen. 1997. Gated access to the pore of a voltage-dependent K^+ channel. *Neuron.* 19: 175–184.
37. Zhorov, B. S., and V. S. Ananthanarayanan. 1996. Structural model of a synthetic Ca^{2+} channel with bound Ca^{2+} ions and dihydropyridine ligand. *Biophys. J.* 70:22–37.
38. Toyoshima, C., M. Nakasako, H. Nomura, and H. Ogawa. 2000. Crystal structure of the calcium pump of sarcoplasmic reticulum at 2.6 A resolution. *Nature.* 405:647–655.
39. Andersen, O. 1984. Chelation of cadmium. *Environ. Health Perspect.* 54:249–266.
40. Zhorov, B. S., and P. D. Bregestovski. 2000. Chloride channels of glycine and GABA receptors with blockers: Monte Carlo minimization and structure-activity relationships. *Biophys. J.* 78:1786–1803.
41. Cuello, L. G., D. M. Cortes, and E. Perozo. 2004. Molecular architecture of the KvAP voltage-dependent K^+ channel in a lipid bilayer. *Science.* 306:491–495.
42. Mackinnon, R. 2004. Voltage sensor meets lipid membrane. *Science.* 306:1304–1305.